USE OF PUBLISHED EXPERIMENTAL RESULTS TO VALIDATE APPROACHES TO GRAY AND DUCTILE IRON MECHANICAL PROPERTIES PREDICTION

Siddhartha Biswas and Charles Monroe
University of Alabama at Birmingham, Birmingham, AL, USA

Thomas Prucha
MetalMorphasis LLC, Rochester Hills, MI, USA

DOI 10.1007/s40962-016-0126-3

Abstract

Cast iron is one of the most widely used materials in the world. Numerous experiments have been conducted in the last 50 years to develop specific microstructure and properties of cast iron. Chemical composition and processing variables have been studied to obtain optimum properties. Efforts have been made to use experimental variables (composition, cooling rate, liquid treatment) and nondestructive tests to predict cast iron's mechanical properties. Most of these relationships are limited to the small data set conducted by a single research project. Researchers at the University of Alabama at Birmingham have collected published cast iron experimental results from the last 40 years to validate the usability of such relationships with a large set of experimental results. In this study, about 2000 cast iron sample data were collected from literature. Statistical analysis was done to compare predicted mechanical properties and experimental measurements. Mean percentage error and mean absolute error are summarized for the whole dataset and for applicable ranges. This summary provides suggestion for which model would be applicable for specific cast iron.

Keywords: *gray, ductile, mechanical properties, prediction*

Introduction

Mechanical property can be defined as a property that involves a relationship between stress and strain or a reaction to an applied force.[1] The mechanical properties determine the range of usefulness and establish the service life that can be expected. Mechanical properties are also used to classify and identify a material. Strength, ductility, hardness, impact resistance, and fracture toughness are the most common mechanical properties considered. These properties of cast iron are related to the microstructure, which is dependent on process variables such as chemical compositions (carbon equivalent, alloying elements), cooling conditions (section size, pouring temperature, and mold material[2]), liquid treatment (spherodizing, inoculation, holding time) and heat treatment.[3–5] Due to the wide variation of properties resulting from the above-mentioned variables, it is difficult to propose any rigorous expression which would predict the magnitude of a property.[6] Noticeable statistical data scatter is reported even for identical sand-cast gray iron parts from three different foundries.[7] It is desirable to have the capability to predict properties in cast iron to permit conservation of alloys while meeting the desired mechanical property requirements and anticipate process design needed to produce specific properties in new or unfamiliar parts. Researchers over the years have applied various methods such as statistical analyses[6,8,9] (regression, separation of variables) of experimental data,[10] numerical analysis,[11,12] artificial neural network (ANN),[13–16] nondestructive tests[17,18] to study these variables to correlate and predict microstructure and mechanical properties. In general, these efforts can be classified into two broad approaches—(a) correlation of process variables to microstructure and mechanical properties and (b) correlation of mechanical properties.

Statistical analysis is performed generally by collection and organization of experimental data (chemical composition, section thickness) from industrial and/or research laboratory cast iron heats. The data were interpreted, correlated,

and presented as a mathematical equation. The predictive analyses are performed separately for ductile and gray iron by the researchers. One of the earliest such work was done by McElwee and Schneidewind[6] to correlate between properties (tensile and compressive strength, Brinell hardness number (HB), modulus of rupture) of gray iron. McElwee and Schneidewind also proposed the tensile strength (TS) prediction model as a function of composition and section thickness. Modification was published on the previously mentioned relationship between gray iron chemistry and tensile strength by Bates[8] and then Shturmakov and Loper.[19] Such multiple regression equation models for ductile iron have been published by researchers.[9,20,21] Graphical representations (contour plots) were published showing combined effects of 11 elements (C, Si, Mg, Ce, Sn, Pb, Ti, Bi, Sb, Cu and Cr) on ductile iron properties.[22]

Numerical analysis creates, analyzes, and implements algorithms for solving the problems of microstructure evolution numerically. Numerical simulations of different processes have seen an extensive and increasing effort due to the advent of computation capability in recent times. Commercial software packages are available to calculate cooling curves, flow rate, and solidification processes. The output of such microstructure evolution is used to predict final microstructure, properties, and quality of final castings.[12] The uses of such software packages are still limited because of the expense and proprietary calculation methodology involved. In literature, researchers have applied thermal analysis and phase growth kinetics within numerical analysis to predict microstructure.[23] The output of these numerical models is used to calculate mechanical properties.[11,21] Mampaey[10] proposed a two-step TS prediction method for any location of a casting. In the first step, TS is calculated based on calculated solidification time. In the second step, influence of the cooling rate during the eutectoid transformation is used to adjust TS calculated in the first step.

Artificial neural network (ANN) is described as mathematical models which solve by means of learning rather than by specific programming based on well-defined rules. ANN has been utilized by researchers to investigate the possibility of predicting mechanical properties. Input variables (composition, inoculation temperature, holding time, casting modulus, etc.) and the output parameter (mechanical properties) are used for training the ANN. A multilayer network with nonlinear perceptrons (functions that can decide whether an input belongs to one class or another) was applied to predict output based on the training. The principle drawback of this method is that the resultant output is specific to training dataset. Also, there is no applicable mathematical relation available in the literature to test the applicability of such ANN method to a different set of experimental data set.

Nondestructive evaluation (NDE) techniques such as ultrasonic velocity,[24] Brinell hardness (HB) measurements,[17] density measurements,[18] and eddy current[25] have been applied to identify different types of cast iron microstructures and correlated with its properties. Cast iron is essentially a mixture of graphite in a matrix of ferrite, pearlite, or carbides. Since graphite has a much lower density compared to other phases, it affects the alloy density directly. Li et al. used this assumption and density measurements of ranges of gray and ductile irons to evaluate cast iron microstructures.[18] Researchers have used ultrasonic and resonance techniques and investigated correlations between acoustic response and certain mechanical properties.[26–31] HB measurements have been correlated by Basaj and Dorn[17] with tensile and yield strength and percent elongation.

The mechanical property prediction methods mentioned above compares very well (R^2 value of at least 0.8) with experimental results compared in respective publications. However, the prediction methodologies in general have been established by using a limited set of laboratory experiments or data from few foundries. Therefore, the question arises: Are these relationships universally applicable to all cast iron foundries? This article will concentrate on validating those relationships with a diverse set of data from sources of different time and production set up.

Methodology

Data Collection

Experimental results of about 2000 heats on cast iron have been collected from literature and internal pours at The University of Alabama at Birmingham (UAB)[32] and the Southern Research Institute (SRI).[33] Cast irons were classified in three categories namely gray (GI), compacted (CGI), and ductile (DI). These categories were specified by the authors of the publications reviewed. The authors of this paper did not make any judgment on determining cast iron classification.

The American Foundry Society (AFS) Transactions have become a rich source of such experimental data over the years.[34–110] Figure 1 shows the distribution of number of AFS Transactions papers and heats reported from 1971 to 2014 from when data was collected. Chemical composition, experimental variables, microstructure analysis, and physical, mechanical, thermal and acoustic properties were tabulated using a spreadsheet. Heat-treated cast iron results were not included in this study. The prediction models available in the literature applicable to only as-cast samples have been considered for this study. Details on the methodology followed in collecting, storing, and categorizing the data has been published by the authors previously.[111] It was also shown that the experimental results

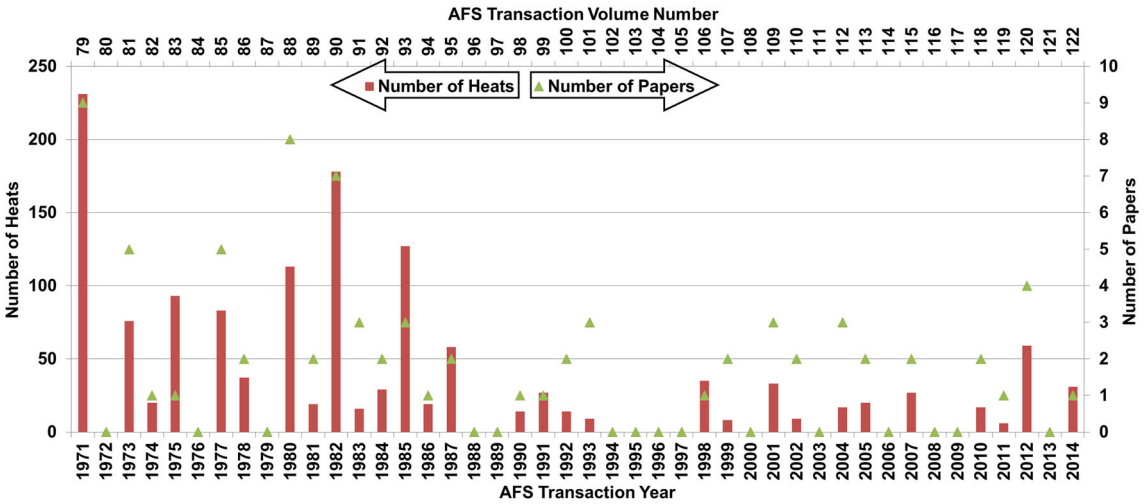

Figure 1. Timeline of data collected from AFS transactions.

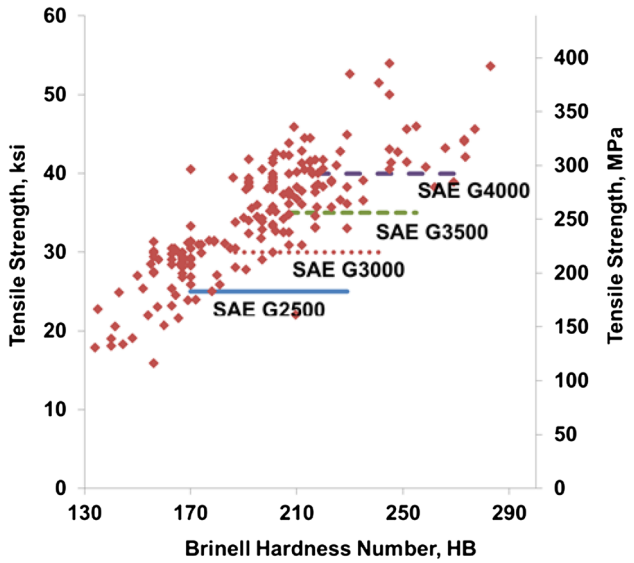

Figure 2. Collected gray iron experimental measurements plotted with SAE standards.

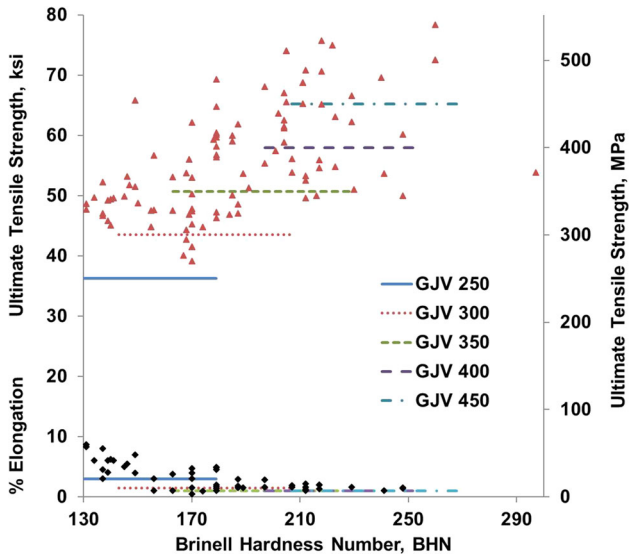

Figure 3. Collected compacted graphite iron experimental measurements plotted with ASTM standards.

collected conform to generally accepted values of chemical composition and mechanical properties. The exceptions can be attributed to experimental variability and measurement techniques.

Available standards generally list minimum acceptable values of tensile strength, yield strength, and percent elongation for each grade of cast iron. A range of HB values expected to have similar strength, and elongation minima as equivalent standard grades are also available. The collected database for this paper is compared with the Society of Automotive Engineers (SAE) standards for GI[112] in Figure 2 and the American Society for Testing and Materials (ASTM) standards for CGI and DI[113,114] in Figures 3 and 4. These figures illustrate the reliability and breadth of the collected data. They also show results which does not conform to any available standard grades. Such results come from research publications dedicated to identify the effect of different casting condition variables over the years. The range of chemical composition and section size is tabulated in Table 1. To summarize, it can be said that the database not only covers industrially accepted values but also includes highs and lows of mechanical properties due to different casting variables.

Analysis

A literature review was made to find mechanical property and microstructure prediction models. Mathematical models with a proposed mathematical equation to predict properties were considered for study in this article.

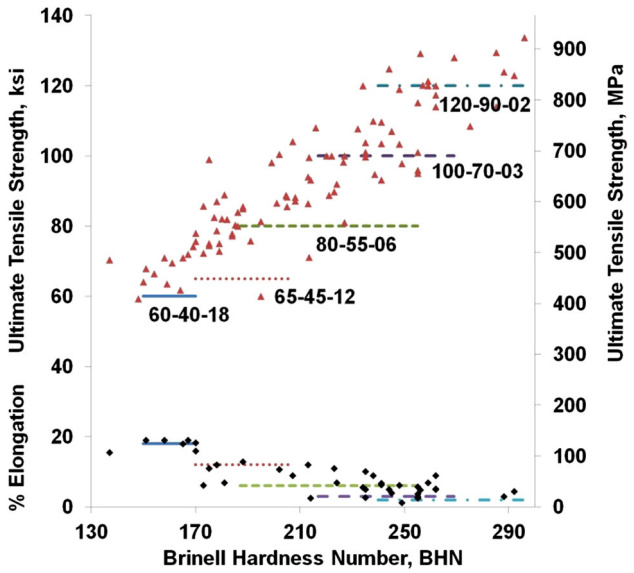

Figure 4. Collected ductile iron experimental measurements plotted with ASTM standards.

Mathematical equations from different methods/models have been used to calculate mechanical properties by using experimental values from the database compiled by the authors of this paper.

Models[11,21] with variables (such as cooling rate of the casting at 900 °C) which are generally not measured are computed using commercially available software.

When using a reference model, data from that article was not included for the analysis. The residual (the difference between the observed value of the dependent variable and the predicted value) was calculated for each data point to find outliers. Outliers are values that fall outside of an overall trend in the data. Sometimes they are caused by error. Other times outliers indicate the presence of a previously unknown phenomenon.

A boxplot, sometimes called a box and whisker plot, was plotted for each set of residuals from the individual model. An example is shown in Figure 5. A boxplot splits the data set into quartiles. The body of the boxplot consists of a "box" (hence, the name), which goes from the first quartile (Q1) to the third quartile (Q3). Within the box, a horizontal line is drawn at the Q2, the median of the data set. The lower and upper limits of acceptable values were calculated using the following equations to identify outliers.

$$\text{Lower limit: } Q1 - 1.5*IQ$$
$$\text{Upper limit: } Q3 + 1.5*IQ$$
$$\text{where IQ} = \text{interquartile range} = Q3 - Q1$$

Two vertical lines, called whiskers, extend from the top and bottom of the box. The top whisker goes from Q3 to the upper limit of nonoutlier in the data set, and the bottom whisker goes from Q1 to the lower limit of nonoutlier.

Outliers were then checked for errors from documentation mistakes, unit conversion and not reported input values

Table 1. Range of Chemical Composition and Section Size (Sample Thickness or Bar Diameter) in the Database Used for Analysis in this Article

	Composition range (%)		
	Gray	Compacted	Ductile
C	1.48–4.16	3.03–4.16	2.95–4.18
Si	0.87–4.00	0.31–4.00	1.21–5.23
P	0.007–0.78	0.008–0.14	0.0014–0.05
CE	2.18–5.13	3.63–4.70	3.69–5.21
Mn	0.01–1.26	0.01–1.09	0.008–1.28
S	0.003–0.4	0.001–0.14	0.001–0.023
Cr	0.02–0.98	0.02–0.239	0.01–0.31
Ce	0.006–0.086	0.001–0.113	0.0–0.049
Cu	0.002–1.06	0.027–3.00	0.01–2.08
Sn	0.002–0.35	0.006–0.5	0.002–0.27
Ni	0.00–1.62	0.01–0.21	0.08–4.15
Mo	0.002–0.78	0.006–0.9	0.00–0.99
Al	0.001–1.98	0.003–5.67	0.008–0.028
Ti	0.00–0.67	0.001–0.58	0.003–0.105
V	0.004–0.51	0.002–0.014	0.001–0.01
Section size, in (mm)	0.5–2.0	0.6–2.0	0.5–2.0
	(12.7–50.8)	(15.2–50.8)	(12.7–50.8)

which would give a false prediction. If no error was detected, the outliers were not discarded. An average value of the residual which is called mean absolute error for each model is reported in Tables 4 and 5. Finally, percentage error was calculated for each data point using Eqn. 1. Mean absolute error (MAE) and mean percentage error of all the analyzed models are summarized in Tables 4 and 5.

$$\text{MAE} = |\text{calculated} - \text{measured}| \quad \text{Eqn. 1}$$

$$\%\text{Error} = \frac{|\text{calculated} - \text{measured}|}{|\text{measured}|} \times 100\% \quad \text{Eqn. 2}$$

If the authors of the specific model specify the applicability range, a similar study as stated above was done within the specified range.

Results

This section summarizes description of test conditions of the sample set for different model, comparative results and statistical variation. Comparisons between experimental and predicted properties by various authors are done in this section. The comparative results within specified applicability range are shown by a solid black circle. The results are shown for gray and ductile iron and arranged chronologically.

Gray Iron Property Prediction

Prediction of gray iron mechanical properties is a complex proposition. Researchers have been utilizing different process variables to propose models which capture the scattering of properties accurately. Most of the models use chemical composition and section size or cooling rate, but there are exceptions too. Jura et al.[115] published a mathematical equation correlating Brinell hardness number (HB) of unalloyed gray cast iron with several parameters of cooling curves. Goettsch et al.[23] developed a gray iron microstructure prediction model base on growth kinetics of gray cast iron. Hua-Qin et al.[116] published a tensile strength prediction model based on inoculants containing Rare Earth, Al, Ca, Cu, Cr, Mn, and Si. In this section, gray iron properties prediction models with mathematical equation with commonly measured and reported variables are studied.

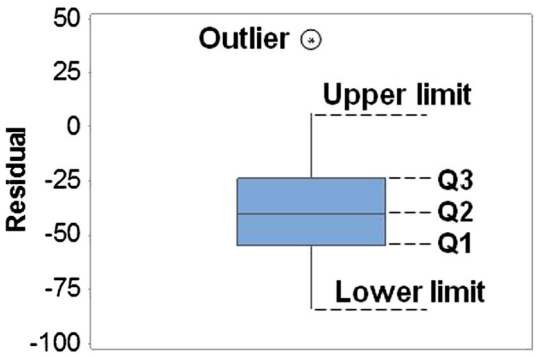

Figure 5. Schematic of box and whisker plot.

The first gray iron model studied in this article was published in 1950 by McElwee and Schneidewind.[6] They developed a tensile strength (TS) prediction method for selection of alloy additions necessary to meet requirements of critical casting sections. The method was expressed as the following equation:

$$\text{TS (ksi)} = 10(b - 2(\%\text{CE}))(f_1)(f_2)(f_3)\ldots(f_n) \quad \text{Eqn. 3}$$

where b is a constant depending on section size; C.E. is carbon equivalent; and the fs are multiplying factors for the alloys. The factors can be read off from the plot of alloy factor as a function of percent alloy in the article (Figure 6). The predicted TS is compared with experimental measurements in Figure 7. The mean percentage error was calculated to be ±11.5% for the complete database.

They also suggested a rapid approximation of tensile strength (in psi) based on a given section size, D (in inches) and carbon equivalent. For unalloyed gray cast iron, the equation is expressed as:

$$\text{TS (ksi)} = 10(11.68 - 2(\%\text{CE})) - 2.3\log D \quad \text{Eqn. 4}$$

The simplified equation was used to compare the model prediction with the experimental tensile strength measurement collected in the database. The comparison is shown in Figure 8. Surprisingly, this model had the least mean percent error (±11%) among all the models compared.

Bates[8] at Southern Research Institute (SRI) developed multiple regression equations based on experiments on gray iron. Eleven heats of cast iron were produced to determine the effect of individual ally elements and section size on mechanical properties. The iron was poured at a

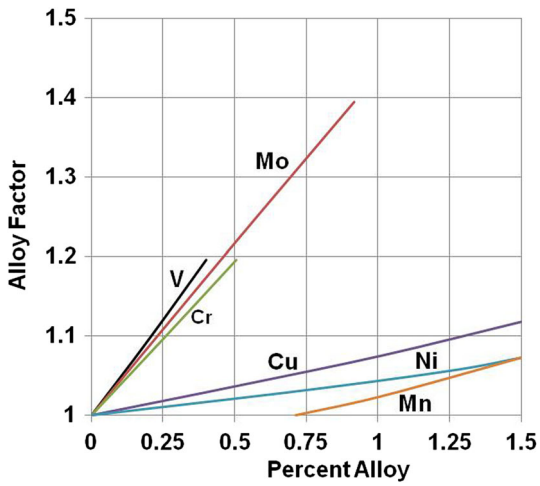

Figure 6. Multiplication factors for McElwee tensile strength prediction model (reproduced from Reference 6).

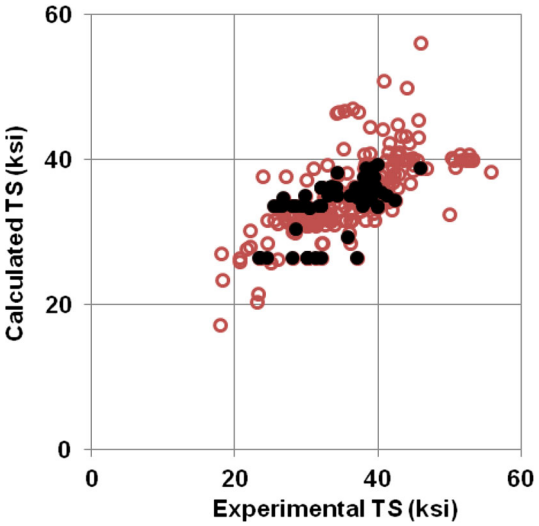

Figure 7. Comparison of values of tensile strength measured versus predicted by McElwee and Schneidewind using alloy addition factors.

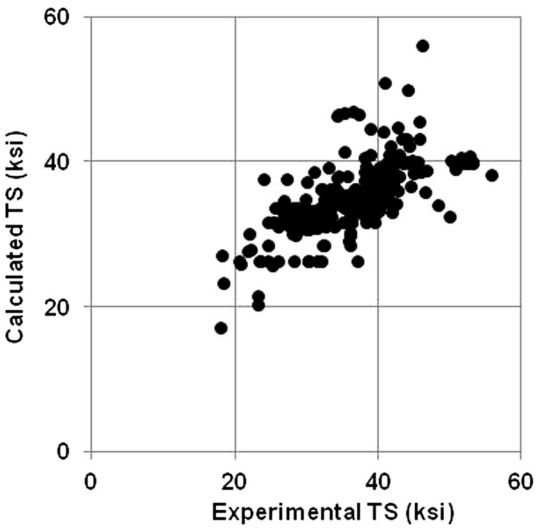

Figure 8. Comparison of values of tensile strength measured versus predicted by McElwee and Schneidewind.

temperature of 2500–2525 °F. Four 0.875-in-diameter "A" bars, six 1.2-in-diameter "B" bars, and a 2-in-diameter "C" bar were poured from each heat. The following correlation equation between strength and yield strength to the chemical compositions and sample diameter was proposed after statistical analysis.

$$\begin{aligned}\text{TS (ksi)} = {} & b_0 + b_1(\%\text{C}) + b_2(\%\text{Si}) \\ & + b_3(\%\text{Mn} - 1.7(\%\text{S}) + b_4(\%\text{Cr}) + b_5(\%\text{Ni}) \\ & + b_6(\%\text{Cu}) + b_7(\%\text{Mo}) + \frac{b_8}{\text{dia(in)}} \\ & + b_9(\%\text{Si})^2 + b_{10}(\%\text{Cu})^2 + b_{11}(\%\text{Mo})^2\end{aligned} \qquad \text{Eqn. 5}$$

The values of coefficients (b's) for tensile and yield strength and limiting ranges of chemical composition and sample diameter for the use of this equation are reported in Tables 2 and 3, respectively.

The comparison between Bates model and experimental measurements is shown in Figure 9. The percentage error was calculated to be ±24% for the complete dataset and also within the specified range.

Yang et al.[117] expressed experimental measurements of HB (Eqn. 6) and percent pearlite content (Eqn. 7) relative to various alloying elements and cooling rate. A total of 16 experimental heats were melted in an induction furnace, and five sample cylinders with varying diameters and standardized tensile test bar were cast. Cooling curve data was recorded, and first- and second-order polynomial approximation of each was constructed. Cooling rate at 900 °C and composition were correlated with hardness and percent pearlite. The equations obtained are shown below.

Table 2. List of Coefficients for Bates Gray Iron Prediction Model (Reproduced from Reference 8)

	TS	YS
b0	162.379	94.25184
b1	−21.7853	−15.3045
b2	−61.2982	−21.3698
b3	−10.5943	−6.61201
b4	13.80529	14.03111
b5	2.056516	3.211982
b6	30.66891	20.209
b7	39.7538	22.5846
b8	16.61308	12.89188
b9	14.16389	4.671514
b10	−26.2518	15.60857
b11	−23.8351	−9.76298

Table 3. Applicable Condition for Bates Regression Equation (Reproduced from Reference 8)

	Range	
C	3.04	3.29
Si	1.6	2.71
S	0.089	0.106
Mn	0.39	0.71
Cr	0.1	0.55
Ni	0.07	1.62
Cu	0.07	0.85
Mo	0.05	0.78
Sn	0.01	0.12
Bar dia (in)	0.875	2

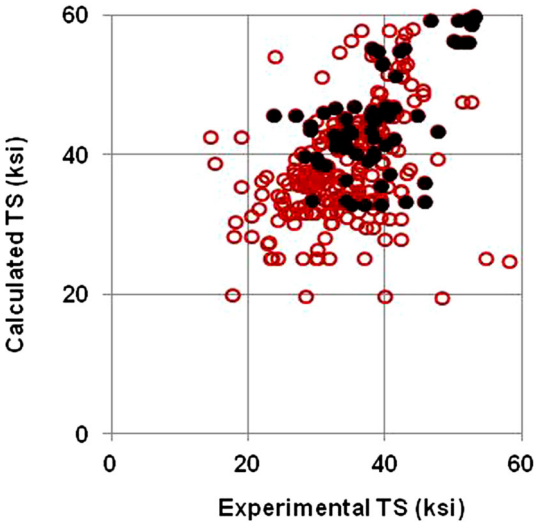

Figure 9. Comparison of values of tensile strength measured versus predicted by Bates et al.

$$\begin{aligned}\text{HB} = {} & 106.7 + 111(\%\text{Cr}) + 508(\%\text{Cr})^2 + 150.8(\%\text{V}) \\ & - 96(\%\text{V})^2 - 93.7(\%\text{Mo}) \\ & + 167.36(\%\text{Mo})^2 + 20.7(\%\text{Cu}) - 10.6(\%\text{Ni}) \\ & + 74.1(\nu 900) - 15.3(\nu 900)^2\end{aligned} \qquad \text{Eqn. 6}$$

$$\begin{aligned}\%\text{Pe} = {} & 63.3 + 90.8(\%\text{Cr}) - 93.1(\%\text{Cr})^2 + 60.9(\%\text{V}) \\ & - 126.4(\%\text{V})^2 - 174.9(\%\text{Mo}) \\ & + 199.6(\%\text{Mo})^2 + 25.7(\%\text{Cu}) + 9.4(\%\text{Ni}) \\ & + 25.2(\nu 900) - 6.8(\nu 900)^2\end{aligned} \qquad \text{Eqn. 7}$$

$$\begin{aligned}\nu 900 &= \text{cooling rate at } 900\ ^\circ\text{C} \\ &= 0.4283(\text{modulus, cm})^2 - 2.0444\end{aligned} \qquad \text{Eqn. 8}$$

A linear regression was done between tensile strength and hardness.

$$\text{TS(ksi)} = \frac{-3.2997 + 1.4335\text{HB}}{6.89}; \quad [R^2 = 0.94] \qquad \text{Eqn. 9}$$

The comparative results between prediction and measurement of hardness are shown in Figure 10 and of tensile strength is shown in Figure 11. Cooling rate at 900 °C for different section sizes were calculated using a regression curve fitting the equation obtained from a commercially available solidification software package. The details are described in the "Appendix".

Bates[118] work modified the tensile strength model of McElwee. The effects of alloying elements were adjusted, and the following equations were reported. The calculated tensile strength results are compared in Figure 12.

$$\text{TS} = \text{A} \times \text{B} \qquad \text{Eqn. 10}$$

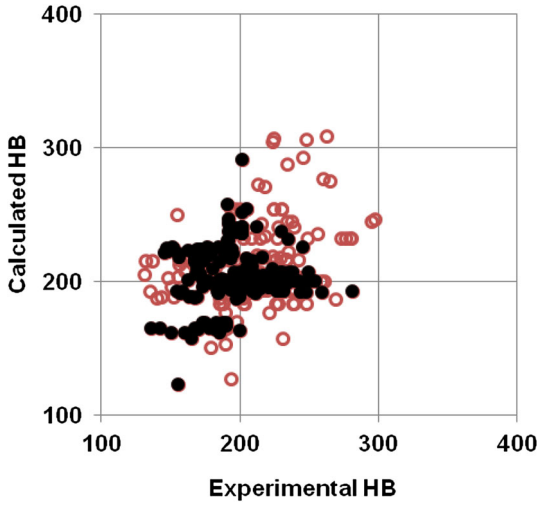

Figure 10. Comparison of values of hardness measured versus predicted by Yang et al.

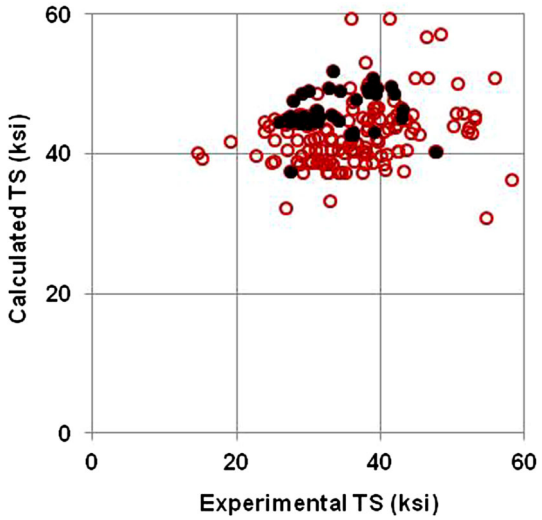

Figure 11. Comparison of values of tensile strength measured versus predicted by Yang et al.

where

$$\begin{aligned}A = {} & 101.1193 - 20.3283((\%\text{C}) + (\%\text{Si})/4 + (\%\text{P})/2) \\ & + 4.3887/(\text{cast bar radius})\end{aligned}$$

$$\begin{aligned}B = {} & 1.000 + 0.1371(\%\text{Si}) - 0.0021((\%\text{Mn}) - 1.7(\%\text{S})) \\ & - 0.3132(\%\text{S}) + 0.3562(\%\text{Cr}) + 0.0282(\%\text{Ni}) \\ & + 0.1107(\%\text{Cu}) + 0.6297(\%\text{Mo}) - 5.2985(\%\text{Ti}) \\ & - 0.2305(\%\text{Sn})\end{aligned}$$

Shturmakov and Loper[19] used mechanical property and chemical composition data from a commercial gray iron (ASTM classes 30B, 35B and 40B) foundry to evaluate by means of multiple regression, using the least squares method. Samples were melted in a cupola furnace and tapped into a channel holding furnace and then transferred to a pouring ladle. A total of 3117 test ASTM B bars were cast to be evaluated, and from the analysis the following predictive equations for hardness and tensile strength were obtained.

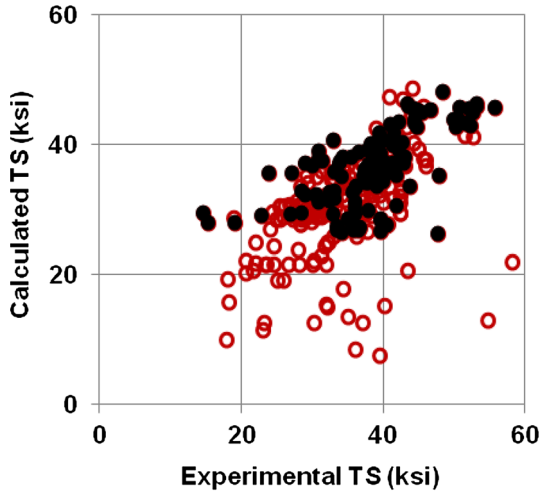

Figure 12. Comparison of values of tensile strength measured versus predicted by modified model of McElwee by Bates et al.

$$\begin{aligned}HB = {} & 470 - 77.6(\%C) - 15.8(\%Si) + 52.7(\%Mn) + 65.2(\%S) \\ & + 69.3(\%P) + 45.8(\%Cr) - 5.2(\%Ni) + 28.8(\%Cu) + 102(\%Al) \\ & - 971(\%Ti) - 109(\%V) + 71.6(\%Sn) + 101(\%)Mo\end{aligned} \quad \text{Eqn. 11}$$

$$\begin{aligned}TS = {} & 157.176 - 32.031(\%C) - 4.388(\%Si) \\ & - 1.427(\%Mn) + 16.653(\%S) - 3.524(\%P) \\ & + 9.675(\%Cr) - 3.768(\%Ni) + 2.419(\%Cu) \\ & + 69.209(\%Al) - 220.366(\%Ti) - 30.383(\%V) \\ & - 9.520(\%Sn) + 13.619(\%Mo)\end{aligned} \quad \text{Eqn. 12}$$

The equations were used for calculating hardness and tensile strength for the database collected by the authors of this article. The calculated results are compared in Figure 13 for tensile strength and in Figure 14 for hardness. The range of hardness and strength cast iron samples used to formulate the equations by Shturmakov and Loper is applied, and the comparative results are shown with solid black circle in Figures 13 and 14.

The mean percent error analysis shows an error of ±20% for hardness and ±24% for tensile strength. Application of the applicable range improved the prediction results by approximately ±2%.

The results of the statistical analysis to compute mean percent error and mean absolute error are summarized in Table 4. The results are also listed for available application range specified with the respective model.

Ductile Iron Property Prediction

The application of ductile iron (DI) is increasing more and more due to its excellent properties and castability. Microstructural factors such as nodularity of graphite, nodule count, matrix microstructure, and presence of nonmetallic inclusions determine properties of DI castings.

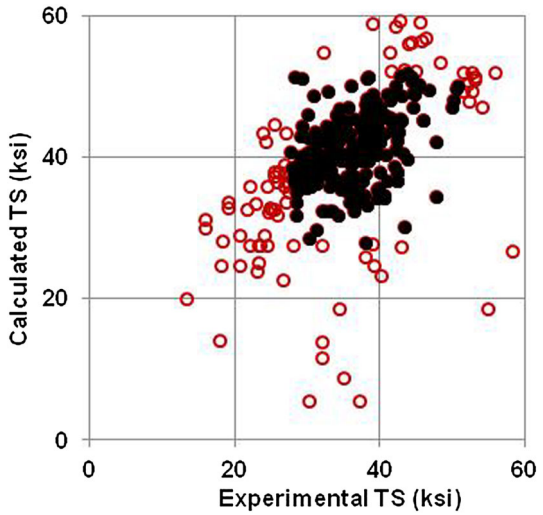

Figure 13. Comparison of values of tensile strength measured versus predicted by Shturmakov and Loper.

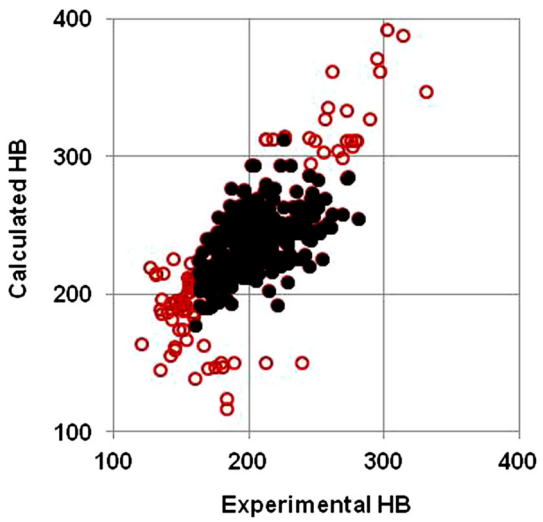

Figure 14. Comparison of values of hardness measured versus predicted by Shturmakov and Loper.

Microstructure is dependent on composition, inoculation treatment, and cooling rate. A large number of researchers have studied possible ways of predicting mechanical properties based on the above-mentioned variables. In this section, the published models are introduced and then a comparative analysis is done with the database collected by the authors of this article.

Yu et al.[20] studied the effects of alloying elements (Mo, Ni, Cu) on HB of ductile iron. In total, 19 DI heats were produced to cast cylindrical bars of five different diameters. The hardness measurements were taken from the center of the bar. A ductile iron HB prediction model was proposed based on regression analysis of chemical composition and section size (D) in inches. A similar equation to predict percent ferrite (f_α) present in the casting was also

Table 4. Summary of the Statistical Analysis of Comparisons Between Prediction Models and Experimental Measurements for Gray Iron

Reference	Predicted property	Input variables	Complete database		Applicability range as reported	Within specified range	
			Mean % error	Mean absolute error		Mean % error	Mean absolute error
McElwee and Schneidewind Unalloyed[6]	TS (ksi)	Composition, section size	11.7 ± 9.2	4.1 ± 3.4	–	–	–
McElwee and Schneidewind[6]	TS (ksi)	Composition, section size	11.5 ± 9.1	4.1 ± 3.3	Alloy ranges in Figure 6	10.3 ± 7.3	3.4 ± 2.3
Bates[8]	TS (ksi)	Composition, section size	24.1 ± 21.4	8.2 ± 6.3	Listed in Table 3	24.3 ± 16.9	9.2 ± 5.2
Bates 91[118]	TS (ksi)	Composition, section size	15.0 ± 16.4	5.5 ± 7.1	Pearlitic	13.3 ± 14.5	4.7 ± 3.8
Yang[117]	HB	Composition, cooling rate	15.6 ± 12.1	29.8 ± 20.5	130–280	14.4 ± 11.3	27.3 ± 19.4
Yang et al.[117]	TS (ksi)	Composition, cooling rate	31.4 ± 26.3	10.1 ± 6.8	22–58	41.8 ± 18.4	13.0 ± 4.5
Shturmakov and Loper[19]	HB	Composition	19.5 ± 12.0	37.1 ± 21.0	HB 160-289	18.3 ± 11.0	36.2 ± 21.0
Shturmakov and Loper[19]	TS (ksi)	Composition	23.8 ± 18.8	8.1 ± 6.9	TS 27.6-51.1	21.1 ± 15.8	7.4 ± 5.4

published. It was reported that HB is related exponentially with percent pearlite content (f_{Pe}). The published equations to calculate percent ferrite and hardness are shown below.

$$f_\alpha = 15.6 - 11.9(\%\text{Mo}) - 13.6(\%\text{Cu}) + 19(D) - 8.1(\%\text{Ni})(D) - 15.9(\%\text{Cu})(D) \quad \text{Eqn. 13}$$

$$\text{HB} = 237 + 151(\%\text{Mo}) + 68.4(\%\text{Ni}) + 89(\%\text{Cu}) - 21.3(D) - 51.7(D)(\%\text{Mo}) - 20.4(D)(\%\text{Ni}) \quad \text{Eqn. 14}$$

$$\text{HB} = \exp(5.01 + f_{Pe}) \quad \text{Eqn. 15}$$

The experimental measurements were reported to be scattered for castings with over 90% pearlite. Once the matrix is fully pearlitic, or nearly so, hardness is affected by solid solution strengthening and pearlite fineness. Yu et al. prediction model was applied to calculate hardness and then compared in Figure 15. Hardness prediction was also done for castings with pearlite content <90% and is shown with solid black circles in figure. Equation 14 was not included in the figure because the agreement was poor.

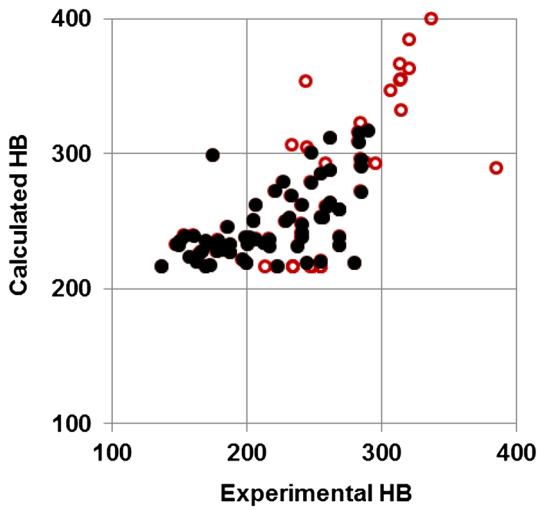

Figure 15. Comparison of values of hardness measured versus predicted by Yu et al. (Eqn 14).

Venugopalan and Alagarsamy[9] investigated the effects of chemical composition and microstructure on the mechanical properties of ductile iron. Their study consisted of 15 different experimental ductile iron castings. Base iron was melted in a commercial cupola and then treated with Mg–Fe–Si alloy containing 0.5% cerium by the sandwich method in a tundish ladle before pouring keel blocks (1 × 1.5 × 8 in legs) and Y blocks (with 1 × 2 in legs) in green sand molds. Chemical composition (C, Si, Mn, P, Cu, Ni, and Mo) of the irons were varied to create ductile iron with varying ferrite in the matrix microstructure. Linear multiple regression equations, one including phosphorus content as an independent variable (Eqn. 16) and one without (Eqn. 17), were generated from the results to the predicted percent of ferrite from the experimental measurements.

$$f_\alpha = 66(\%\text{Si}) + 721(\%\text{P}) + 226(\%\text{Mo}) - 29(\%\text{Mn}) - 100(\%\text{Cu}) - 16.5(\%\text{Ni}) - 234(\%\text{Mo})(\%\text{Ni}) - 113(\%\text{Cu})(\%\text{Mo}) - 86 \quad \text{(Eqn. 16)}$$

$$f_\alpha = 69(\%Si) + 198(\%Mo) - 35(\%Mn) - 109(\%Cu) - 22(\%Ni) - 202(\%Ni)(\%Mo) - 74(\%Cu)(\%Mo) - 73 \quad \text{Eqn. 17}$$

Vickers indenter was used to measure micro hardness of the matrix phases with a 100-gf load. Knoop indenter was used when the ferrite ring thickness was too small. Ferrite and pearlite microhardness measurements were then fitted in multiple regression equations with the composition. The simple rule of mixture was utilized to get the composite matrix micro hardness (CMMH). Finally, CMMH was used in linear regression expressions to get tensile strength, yield strength, and elongation prediction equations shown below.

$$\text{Ferrite hardness(HF)} = 64 + 44(\%Si) + 9(\%Mn) + 114(\%P) + 10(\%Cu) + 7(\%Ni) + 22(\%Mo) \quad \text{Eqn. 18}$$

$$\text{Pearlite hardness(HP)} = 249 + 26(\%Si) + 12(\%Mn) + 234(\%P) + 16(\%Cu) + 17.5(\%Ni) + 26(\%Mo) \quad \text{Eqn. 19}$$

$$\text{Composite matrix micro hardness(CMMH)} = ((\text{HF}) \times (\%f_\alpha) + (\text{HP}) \times (\%\text{Pe}))/100 \quad \text{Eqn. 20}$$

$$\text{TS(ksi)} = 0.10 + 0.36(\text{CMMH}) \quad \text{Eqn. 21}$$

$$\text{YS(ksi)} = 12 + 0.18(\text{CMMH}) \quad \text{Eqn. 22}$$

$$\%\text{EL} = 37.85 - 0.093(\text{CMMH}) \quad \text{Eqn. 23}$$

These equations (which include P as an independent variable) were used to calculate hardness and tensile strength for published experimental compositions of ductile iron. The calculated results were then compared with reported values. The comparisons for Brinell hardness are shown in Figure 16 and for tensile strength are shown in Figure 17. Statistical analyses of the comparisons are shown in Table 5.

In 1993, an equation to calculate Brinell hardness for low alloyed ductile iron from ferrite fraction (f_α) and silicon content was published by Svensson et al.[119] The relationship was developed by using solidification and solid-state transformation modeling. The model takes into account the impacts of silicon addition such as solution hardening effect and increased driving force for ferrite precipitation. These are equations are reported to be valid in the range of 1.7–4.9% silicon.

$$\text{HB} = \left(\text{HB}_\alpha^{(\%Si)}\right)(f_\alpha) + \text{HB}_{\text{Pe}}^{(\%Si)}(1 - f_\alpha) \quad \text{Eqn. 24}$$

$$\text{HB}_\alpha^{(\%Si)} = 54 + 37(\%Si) \quad \text{Eqn. 25}$$

$$\text{HB}_{\text{Pe}}^{(\%Si)} = 167 + 31(\%Si) \quad \text{Eqn. 26}$$

Svensson model was used to calculate hardness for experimental heats with necessary variables available. The comparison between measured and predicted values is shown in Figure 18. Mean percent error reduced from ±8.9 to ±7.1 when applied within the specified silicon range and unalloyed DI castings. It can be seen from Figure 18 that, around above HB 250, the model fails to predict as soon as the effect of alloying element comes into play, which is expected for this simple model.

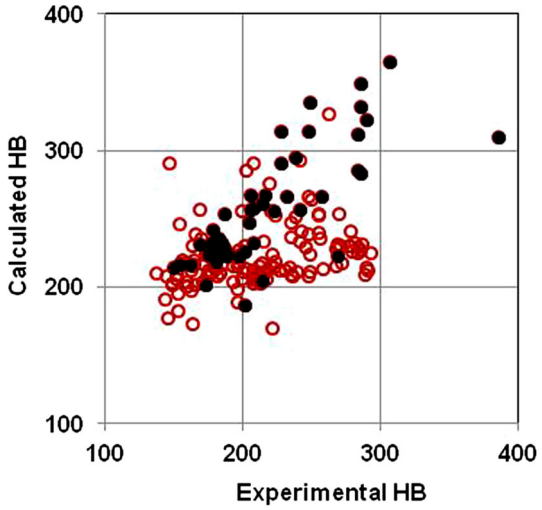

Figure 16. Comparison of values of hardness measured versus predicted by Venugopalan and Alagarsamy.

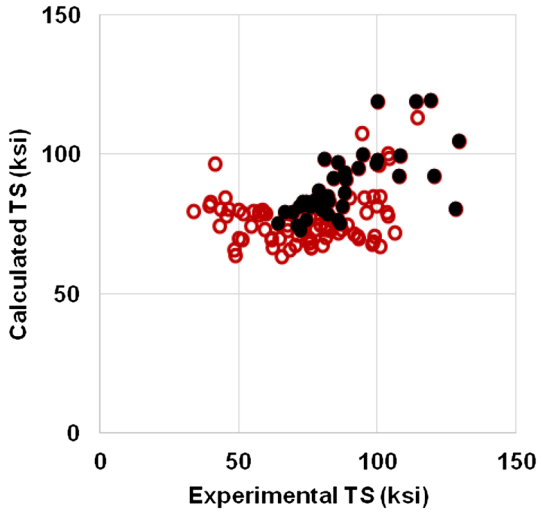

Figure 17. Comparison of values of tensile strength measured versus predicted by Venugopalan and Alagarsamy.

Guo et al.[21] proposed a mechanical property prediction model by taking microstructural evolution into account and utilizing microstructural features such as fractions of graphite, ferrite, and pearlite, and nodularity of graphite. Regression analysis of the above-mentioned variables was done to achieve the following equations to formulate hardness, tensile strength, and elongation.

$$\text{HB} = 100f_{\text{Gr}} + \text{HB}_\alpha f_\alpha + \text{HB}_{\text{Pe}} f_{\text{Pe}} \quad \text{Eqn. 27}$$

where HB_α and HB_{Pe} are hardness of ferrite and pearlite, respectively, f_{Gr}, f_α, f_{Pe} are the fraction of graphite, ferrite, and pearlite, respectively.

Table 5. Summary of the Statistical Analysis of Comparisons Between Prediction Models and Experimental Measurements for Ductile Iron

Authors [reference]	Predicted property	Input variables	Complete database			Within specified range	
			Mean % error	Mean absolute error	Applicability range as reported	Mean % error	Mean absolute error
Yuet al.[20]	HB	Composition, section size	18.9 ± 15.8	39.8 ± 28.0	Pearlite <90%	19.9 ± 16.9	37.9 ± 25.9
Venugopalan and Alagarsamy[9]	TS (ksi)	Composition	20.8 ± 26.0	13.5 ± 11.9	68–124 ksi	9.3 ± 7.8	8.5 ± 9.0
Venugopalan and Alagarsamy[9]	HB	Composition	18.6 ± 14.2	36.8 ± 24.7	151–288	21.6 ± 10.5	44.7 ± 20.2
Svensson et al.[119]	HB	%Si, ferrite fraction (f_α)	8.9 ± 5.8	21.0 ± 18.9	1.7–4.3% Si, unalloyed	7.1 ± 4.1	13.3 ± 7.9
Guo[21]	TS (ksi)	dT/dt, composition	14.9 ± 10.4	12.7 ± 8.5	65–100 ksi	16.9 ± 10.8	13.2 ± 8.7
Guo et al.[21]	HB	dT/dt, composition	6.5 ± 5.2	14.6 ± 12.8	170–269	6.6 ± 5.6	14.9 ± 13.2
Basaj and Dorn[17]	YS (ksi)	HB	11.2 ± 8.4	6.5 ± 4.7	150–300	–	–
Basaj and Dorn[17]	TS (ksi)	HB	11.0 ± 11.1	8.6 ± 7.1	150–300	–	–

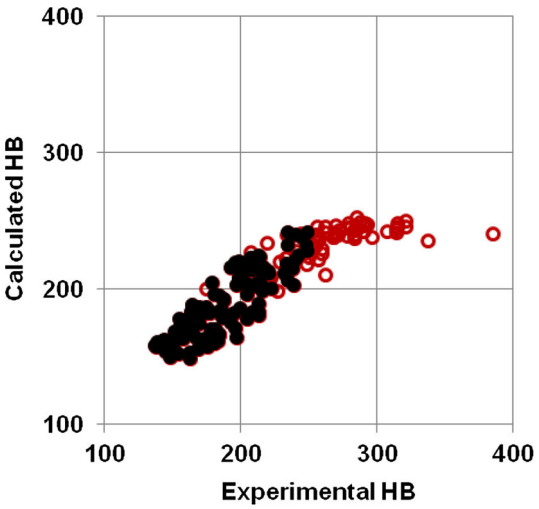

Figure 18. Comparison of values of hardness measured versus predicted by Svensson et al.

$$HB_{Pe} = 223 + 50(\%Mn + \%Cu + \%Cr + \%Mo) + 10(\%Ni) + 20\left(\frac{dT}{dt} - 0.5\right) \quad \text{Equ.28}$$

where, dT/dt = cooling rate at 850 °C.

$$TS(MPa) = \left(1 - f_{Gr}^{n}\right)(482.2f_\alpha + 991.5f_{Pe}) \quad \text{Eqn. 29}$$

$$\%EL = \left(1 - f_{Gr}^{n}\right)(26.2f_\alpha + 5.61f_{Pe}) \quad \text{Eqn. 30}$$

where n is an indication of nodularity. The influence of nodularity was not studied by Guo et al. For their study, n was taken as unity since all samples analyzed by them had good nodularity.

To validate the hardness model, two test castings—one ASTM 65-45-12 and one ASTM 100-70-03 grade having six different diameter cylindrical bars—were poured in resin-bonded sand molds. The tensile strength and elongation model were validated using commercial DI data. Mean percent error was calculated to be ±4.13, ±4.06, and ±9.14, respectively, for hardness, tensile strength, and elongation.

Guo et al. used mechanical properties model to calculate hardness and tensile strength for published experimental results with documented microstructural and compositional values necessary. Cooling rate dT/dt at 850 °C was not available in the database collected by the authors of this article. A commercially available solidification model was utilized to generate cooling rate data. The procedure followed is described in detail in "Appendix." The comparison for hardness is shown in Figure 19 and for tensile strength is shown in Figure 20. Guo et al. model provides tensile strength in MPa. Conversion was done to ksi to accommodate comparison with other models. Statistical analysis showed mean percent error was ±6.5 and ±14.9 for hardness and tensile strength, respectively. The hardness model was found to have the best fit among the models compared in this study.

Basaj and Dorn[17] studied HB and tensile properties from two commercial foundries. Both foundries produce cupola and electric melt process iron. Keel block test bars were produced for hardness and tensile property measurements. Hardness values were obtained using the optical scan measurement of the indentation at the cross section of the tensile bar shank and midway between the center and

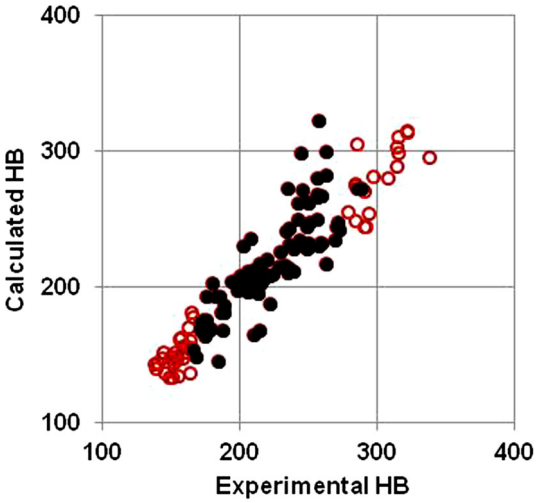

Figure 19. Comparison of values of hardness measured versus predicted by Guo et al.

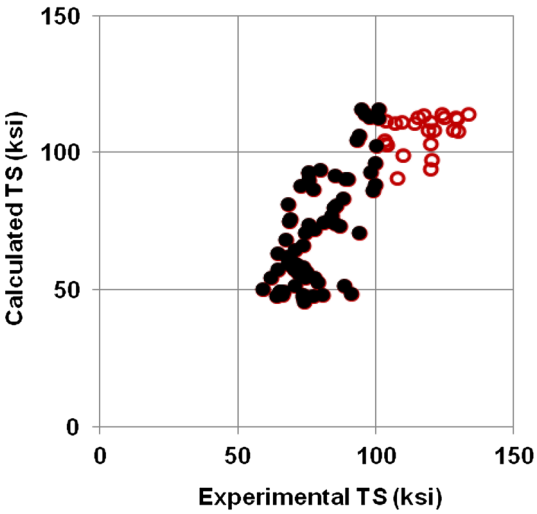

Figure 20. Comparison of values of tensile strength measured versus predicted by Guo et al.

surface. Statistical regression analysis was done to obtain equations to predict tensile properties and percent pearlite from hardness measurements. Two separate set of equations denoted by A and B were obtained to have a better fit for individual foundries. R^2 values in excess of 0.8 were obtained for all the cases. The equations published are shown here.

$$\text{A1}: \ \text{TS(psi)} = 504(\text{HB}) - 13574; \quad \left[R^2 = 0.981\right] \qquad \text{Eqn. 31}$$

$$\text{A2}: \ \text{YS(psi)} = 223(\text{HB}) + 8179; \quad \left[R^2 = 0.92\right] \qquad \text{Eqn. 32}$$

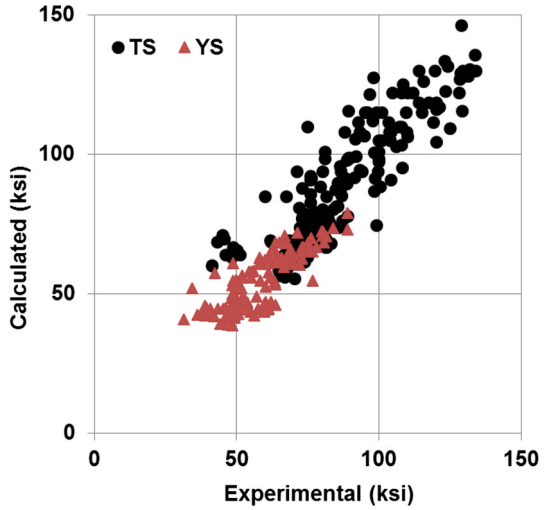

Figure 21. Comparison of values of tensile and yield strength measured versus predicted by Basaj et al.

$$\text{A3}: \ \log(\text{HB}) = 2.44796 + 0.210607\log(\%\text{EL}) - 0.321105(\log \text{EL})2; \quad \left[R^2 = 0.924\right] \qquad \text{Eqn. 33}$$

$$\text{A8}: \ f_{\text{Pe}} = 0.7351(\text{HB}) - 105.3; \quad \left[R^2 = 0.89\right] \qquad \text{Eqn. 34}$$

$$\text{B1a}: \ \text{TS} = 0.4519(\text{HB}) - 4.726; \quad \left[R^2 = 0.93\right] \qquad \text{Eqn. 35}$$

$$\text{B2}: \ \text{YS(ksi)} = 0.2254(\text{HB}) + 8.2557; \quad \left[R^2 = 0.87\right] \qquad \text{Eqn. 36}$$

$$\text{B3}: \ \%\text{EL} = 0.0003(\text{HB})^2 - 0.2401(\text{HB}) + 48.569; \quad \left[R^2 = 0.86\right] \qquad \text{Eqn. 37}$$

$$\text{B5}: \ \%\text{Pearlite} = -0.000084973(\text{HB})^3 + 0.055(\text{HB})^2 - 11.009(\text{HB}) + 715.2; \quad \left[R^2 = 0.83\right] \qquad \text{Eqn. 38}$$

For comparison in this study, equations from foundry A were used. Figure 21 shows the tensile strength and yield strength comparison between experimental measurements and prediction from Basaj et al. models. The strength models were found to have the best fit (least error) within the models studied in this study with mean error ±11%.

The results of the statistical analysis to compute mean percent error and mean absolute error are summarized in Table 5. The results are also listed for available application range specified with the respective model.

Discussion

Comparison Between Models

All the models analyzed above uses positive or negative influence coefficient related to input variables such as chemical composition and section size. Comparison between models is possible by calculating property using same chemical composition. If one of the element composition is varied, the trend or influence of that element on different models can be observed. To obtain such comparative results, copper (Cu) composition was chosen as the varying element. Copper has a distinctive effect on transforming matrix structure from ferritic to pearlitic. And as the percent pearlite increases, mechanical properties such as tensile strength and hardness increases too. Figure 22 shows the effect of increase in percentage pealite in matrix on tensile strength.

The effect of copper addition on mechanical properties and microstructure are well understood. All the models include copper as an input variable. In this study copper composition was varied between zero to one percent. Average composition of ASTM class 40 and ASTM grade 80-65-6 was used, respectively, for gray and ductile iron to calculate tensile strength. The section thickness/bar diameter was kept constant at 1 inch for all the calculations. The compositions used for calculations are given in Table 6.

Figure 23 shows the calculated tensile strengths as lines as a function of copper composition. The black solid dots

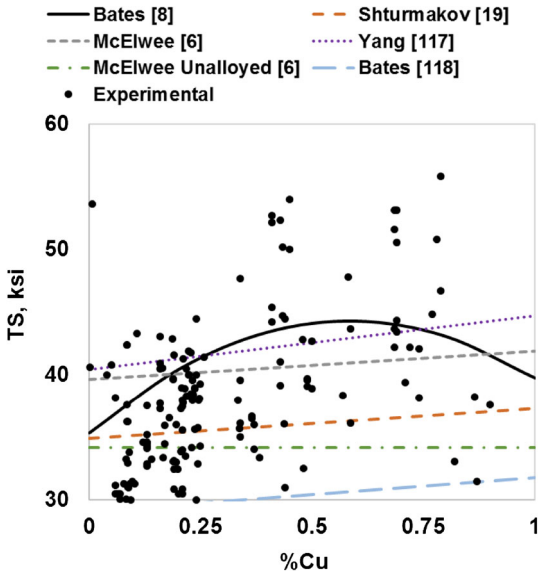

Figure 23. Tensile strength as a function of percentage copper for gray iron.

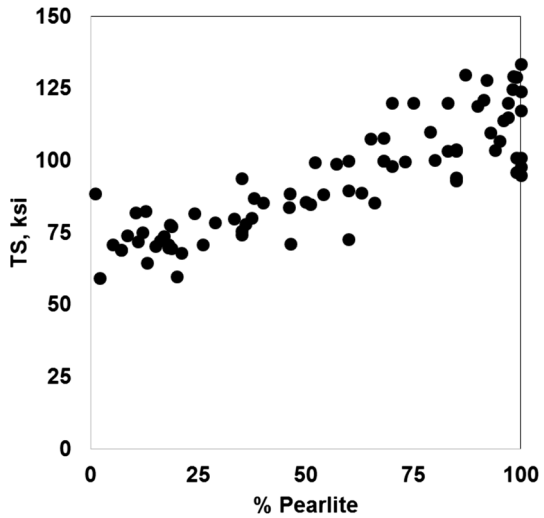

Figure 22. Ductile iron tensile strength as a function of percentage pearlite.

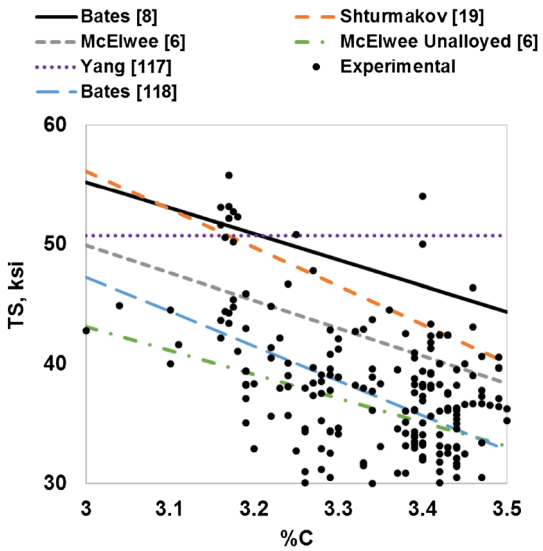

Figure 24. Tensile strength as a function of percentage carbon for gray iron.

Table 6. Iron Composition Used for Comparison Between Property Prediction Models

Iron	Standard	C	Si	Mn	S	P	Mo	Ni	Sn	Cu
Gray	ASTM Class 40	3.42	2.13	0.56	0.076	0.077	0.02	0.024	0.02	0–1.0
Ductile	ASTM 80-65-6	3.70	2.30	0.56	0.005	0.077	0.05	0.125	0.02	0–1.0

represent the measured tensile strength. The composition of the experimental results IS not limited to class 40. All the models, except Bates, show an increase in strength with copper addition. The Bates model predicts a maximum strength and then reduction as more copper is added.

Similar study can be done for other elements. Carbon has a negative effect on strength and is shown in Figure 24. Yang model does not have carbon as input variable and that is why it appears as a flat line on the figure. Carbon composition was varied between 3 and 3.5% and all the other elements were kept constant as stated in Table 6. Copper composition was kept fixed at 0.3%.

In case of ductile iron, average composition of ASTM grade 80-65-6 was used to calculate strength with varying copper percentage. The results are shown in Figure 25.

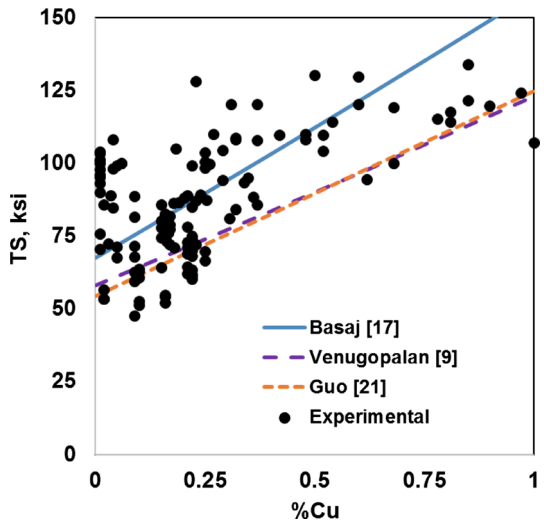

Figure 25. Tensile strength as a function of percentage copper for ductile iron.

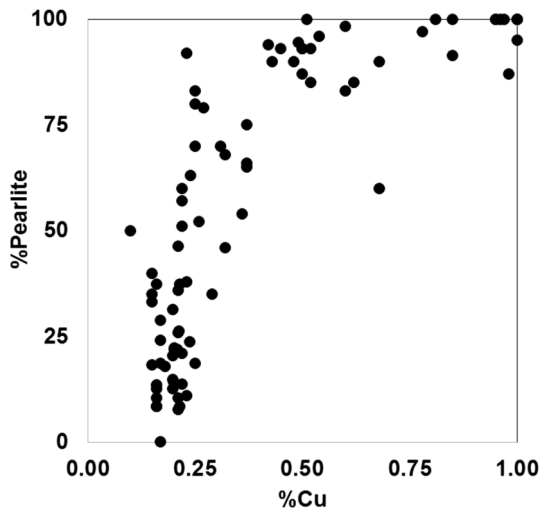

Figure 26. Percent pearlite in microstructure as a function of Copper addition.

Venugopalan and Guo model is shown to overlap. For Basaj model, hardness was used from Venugopalan model. Although all the models predict a linear increase in tensile strength with increase in copper, the experimental measurements shows increase up to 0.5% Cu, and then tensile strength reaches a plateau. Figure 26 shows effect of copper addition on amount of pearlite present in matrix microstructure. Percent pearlite reaches 90–100% with 0.5% copper addition.

The database can be used to conduct similar studies for other variables to improve current property prediction models. Decreasing percentage error would enable use of such models not only to a certain set of samples but to a broader spectrum of cast iron production facilities.

Conclusion

This article studies the capability of published models to predict mechanical properties of cast iron (GI and DI). The prediction results are compared with experimental measurements collected from the literature. The comparison shows promising results with percent error ±25 or less. Property prediction as a function of a measured property had the least error. Industrial cast iron production facilities can conduct a similar study to find an applicable model. Based on the study the following conclusions can be inferred:

- The deviation between measured and predicted values of mechanical properties could be due to testing procedure difference and/or due to lack of variables such as raw materials, melting procedure, pouring temperature, superheat, inoculation amount and method, and magnesium treatment in the models.
- Limiting the statistical analysis within applicable range did not improve percent error in most cases.
- Property prediction models for ductile iron have less percent error compared to gray iron. Improvement in prediction of ductile iron property could be due to consideration of microstructural evolution in ductile iron models.
- The authors could not find any model for compacted graphite iron, which provides simple mathematical expression to be readily useable. There are future research opportunities to come up with such models.
- The database compiled and used by the authors for this article could be used for validation of relationships correlating cast iron composition, process variables and properties.
- Availability of such database of experimental results from diverse sources enables researchers to validate novel ideas without running rigorous experiments.

- It is of utmost importance to establish a standard procedure to document and publish experimental results in a standard tabular form to enable such future studies and improve current property prediction models.

Acknowledgement

The authors would like to recognize the support of the American Foundry Society and funding received from American Metalcasting Coalition (AMC) (Contract No. SP4701-11-D-0025 Subcontract No. 2012-517) Castings Solutions for Readiness: Tools for Streamlining Casting Supply Chains—Casting Alloy Design Selection Tool program funded by the DLA (Defense Logistics Agency).

Appendix

A sample casting, with 0.5-, 1-, and 2-inch-diameter bar (Figure 27), was used to acquire cooling rate values. Solidification only simulation was done to get the cooling rate (dT/dt) at the center of each bar at 850 and 900 °C, respectively, for casting grade GJS 400 and GJL 250. Regression analysis was done to obtain equation to calculate the cooling rate for other thicknesses within

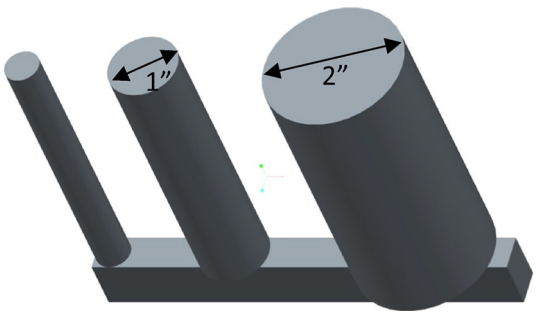

Figure 27. Schematic of the casting design used for cooling rate calculation.

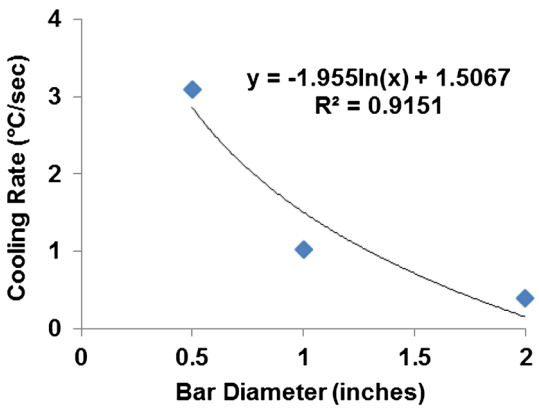

Figure 28. Cooling rate calculation for ductile iron (GJS 400) at 850 °C.

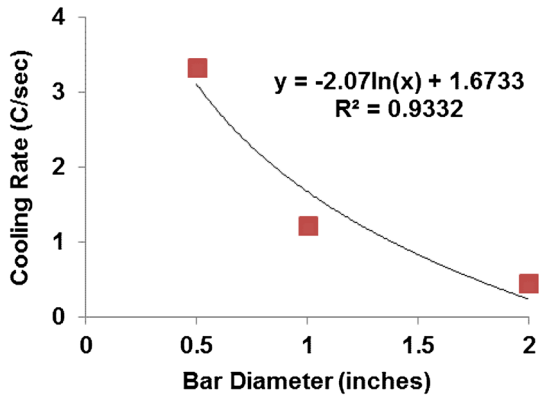

Figure 29. Cooling rate calculation for gray iron (GJL 250) at 900 °C.

0.5 inch to 2 inch. The regression analysis for ductile and gray iron is shown, respectively, in Figures 28 and 29.

REFERENCES

1. http://www.merriam-webster.com/dictionary/mechanical%20property
2. M. Górny, T. Edward, Effect of cooling rate on microstructure and mechanical properties of thin-walled ductile iron castings. J. Mater. Eng. Perform. **22**(1), 300–305 (2013)
3. S. Bockus, Z. Gintautas, Relation between section thickness, microstructure and mechanical properties of ductile iron castings. Mater. Sci. **14**(2), 1392–1420 (2008)
4. S. Bockus, G. Zaldarys, Influence of the section size and holding time on the graphite parameters of ductile iron production. Metalurgija **48**(1), 19 (2009)
5. R.I. El Soeudy, The effect of graphite aspect ratio on the mechanical and microstructural properties of cast iron. Materialwiss. Werkstofftech. **33**(2), 73–79 (2002)
6. R.G. McElwee, R. Schneidewind, Correlation of properties of gray irons. Trans. Am. Foundrymen's Soc. **58**, 323–331 (1950)
7. L. Collini, G. Nicoletto, R. Konecna, Microstructure and mechanical properties of pearlitic gray cast iron. Mater. Sci. Eng., A **488**(1), 529–539 (2008)
8. C.E. Bates, Alloy element effects on gray iron properties. Part II. Trans. Am. Foundrymen's Soc. **94**, 889–912 (1986)
9. D. Venugopalan, A. Alagarsamy, Effects of alloy additions on the microstructure and mechanical properties of commercial ductile iron. Trans. Am. Foundrymen's Soc. **98**, 395–400 (1990)
10. F. Mampaey, Prediction of gray iron tensile strength by the separation of variables. Trans. Am. Foundry Soc. **112**, 879–897 (2004)
11. A. Catalina, X. Guo, D.M. Stefanescu, L. Chuzhoy, M. Pershing, Prediction of room temperature

microstructure and mechanical properties in gray iron castings. Trans. Am. Foundrymen's Soc. **108**, 247–257 (2000)
12. M. Jabbari, D. Parviz, V. Naser, Numerical modeling and experimental validation of microstructure in gray cast iron. Int. J. Miner. Metall. Mater. **19**(10), 908–914 (2012)
13. J. Voracek, Prediction of mechanical properties of cast irons. Appl. Soft Comput. **1**(2), 119–125 (2001)
14. I. Zmak, F. Tomislav, Mechanical properties of ductile cast iron determined by neural networks, in *The Third International Conference on Modeling, Simulation and Applied Optimization* (2009)
15. S. Calcaterra, G. Campana, L. Tomesani, Prediction of mechanical properties in spheroidal cast iron by neural networks. J. Mater. Process. Technol. **104**(1), 74–80 (2000)
16. M. Perzyk, W.K. Andrzej, Prediction of ductile cast iron quality by artificial neural networks. J. Mater. Process. Technol. **109**(3), 305–307 (2001)
17. L.J. Basaj, T. Dorn, Tensile properties continuum with Brinell hardness of as-cast ductile iron. Trans. Am. Foundrymen's Soc. **107**, 671–677 (1999)
18. H. Li, R.D. Griffin, Evaluating cast iron microstructures using density measurements. Trans. Am. Foundry Soc. **111**, 703–714 (2003)
19. A.J. Shturmakov, C.R. Loper, Predictive analysis of mechanical properties in commercial gray iron. Trans. Am. Foundry Soc. **107**, 609–615 (1999)
20. S.K. Yu, C.R. Loper Jr., The effect of molybdenum, copper, and nickel on the pearlitic and martensitic hardenability of ductile cast irons. Trans. Am. Foundrymen's Soc. **96**, 811–822 (1988)
21. X. Guo, D.M. Stefanescu, L. Chuzhoy, M.A. Pershing, G.L. Biltgen, A mechanical properties model for ductile iron. Trans. Am. Foundrymen's Soc. **105**, 47–54 (1997)
22. T. Watmough, W.F. Shaw, F.C. Bock, Combined effects of selected elements on the properties of ductile iron. Trans. Am. Foundrymen's Soc. **79**, 225–246 (1971)
23. David D. Goettsch, Jonathan A. Dantzig, Modeling microstructure development in gray cast irons. Metall. Mater. Trans. A **25**(5), 1063–1079 (1994)
24. J. Griffin, R. Griffin, Compacted Graphite Iron and Ultrasonic Testing, Ductile iron news, issue 2 (2006)
25. S. Konoplyuk, T. Abe, T. Uchimoto, T. Takagi, M. Kurosawa, Characterization of ductile cast iron by eddy current method. NDT and E Int. **38**(8), 623–626 (2005)
26. P.J. Emerson, W. Simmons, Final report on the evaluation of the graphite form in ferritic ductile iron by ultrasonic and sonic testing, and the effect of graphite form on mechanical properties. Trans. Am. Foundrymen's Soc. **84**, 109–128 (1976)
27. A.G. Fuller, P.J. Emerson, G.F. Sergeant, Report on the effect upon mechanical properties of variation in graphite form in irons having varying amounts of ferrite and pearlite in the matrix structure and the use of NDT in assessments of mechanical properties of such iron. Trans. Am. Foundrymen's Soc. **88**, 21–50 (1980)
28. V.B. Kovacs, G.S. Cole, Interaction of acoustic waves with SG (spheroidal-graphite) iron castings, in *Proceedings of the 2nd International Symposium on the Metallurgy of Cast Iron* (1976), pp. 827–840
29. H. Li, R.D. Griffin, L.E. Bates, Gray iron property measurements using ultrasonic techniques. Trans. Am. Foundry Soc. **113**, 687–697 (2005)
30. J. Cech, Measuring the mechanical properties of cast irons by NDT methods. NDT Int. **23**(2), 93–102 (1990)
31. Y.S. Lerner, A.P. Vorobiev, Nondestructive evaluation of structure and properties of ductile irons. Trans. Am. Foundrymen's Soc. **106**, 47–51 (1998)
32. University of Alabama at Birmingham (UAB) internal pour data (1970–2014)
33. Southern Research Institute (SRI) Internal Reports (1978)
34. E. Campomanes, Effects of minute additions of antimony on structure and properties of ductile iron. Trans. Am. Foundrymen's Soc. **79**, 57–62 (1971)
35. T. Watmough, W.F. Shaw, F.C. Bock, Combined effects of selected elements on the properties of ductile iron. Trans. Am. Foundrymen's Soc. **79**, 225–246 (1971)
36. G.S. Cole, G.F. Bolling, The influence of external forces on the solidification of cast irons. Trans. Am. Foundrymen's Soc. **81**, 59–68 (1973)
37. E. Campomanes, R. Goller, Production of cast iron containing intermediate forms of graphite. Trans. Am. Foundrymen's Soc. **83**, 55–62 (1975)
38. D.R. Askeland, S.S. Gupta, Effect of nodule count and cooling rate on the matrix of nodular cast iron. Trans. Am. Foundrymen's Soc. **83**, 313–320 (1975)
39. J.F. Wallace, Effects of minor elements on the structure of cast irons. Trans. Am. Foundrymen's Soc. **83**, 363–378 (1975)
40. G.F. Ruff, J.F. Wallace, Relation between the traverse and tensile strength of GI. Trans. Am. Foundrymen's Soc. **85**, 171–178 (1977)
41. G.F. Ruff, J.F. Wallace, Effects of solidification structures on the tensile properties of gray iron. Trans. Am. Foundrymen's Soc. 1977 AFS Research Reports (1978), pp. 23–46
42. N.K. Datta, Influence of ladle inoculation and holding time on structure and mechanical properties of GI melted in channel furnaces. Trans. Am. Foundrymen's Soc. **85**, 363–370 (1977)
43. N.P. Lillybeck, M.G. McKimpson, An evaluation of graphite shape consistency in CGI-flake from mechanical property data. Trans. Am. Foundrymen's Soc. **85**, 129–132 (1977)
44. A.G. Fuller, Evaluation of the graphite form in pearlitic DI by ultrasonic and sonic testing and the effect of

graphite form on mechanical properties. Trans. Am. Foundrymen's Soc. **85**, 509–526 (1977)
45. J.E. Bevan, W.G. Scholz, Effects of Mo on transformation characteristics and properties of high strength DI. Trans. Am. Foundrymen's Soc. **85**, 271–276 (1977)
46. M.M. Shea, Influence of cooling rate and Mn and Cu content on hardness of As-cast DI. Trans. Am. Foundrymen's Soc. **86**, 7–12 (1978)
47. M.M. Shea, S.T. Holtan, In the mold treatment using elemental magnesium to produce DI. Trans. Am. Foundrymen's Soc. **86**, 13–22 (1978)
48. K.P. Cooper, C.R. Loper Jr., Some properties of compacted graphite cast iron. Trans. Am. Foundrymen's Soc. **86**, 241–248 (1978)
49. B.V. Kovacs, Pearlite stabilization in cast irons. Trans. Am. Foundrymen's Soc. **89**, 79–96 (1981)
50. D.M. Stefanescu, The importance of the La/RE ratio in the production of CGI. Trans. Am. Foundrymen's Soc. **89**, 113–119 (1981)
51. R.J. Smickley, K.B. Rundman, The effect of aluminum on the structure and properties of gray cast iron. Trans. Am. Foundrymen's Soc. **89**, 205–214 (1981)
52. J.H. Doubrava, S.F. Carter Jr., J.F. Wallace, The influence of processing variables on the matrix structure and nodularity of DI. Trans. Am. Foundrymen's Soc. **89**, 229–250 (1981)
53. W.J. Evans, S.F. Carter Jr., J.F. Wallace, Factors influencing the occurrence of carbides in thin sections of ductile iron. Trans. Am. Foundrymen's Soc. **89**, 293–322 (1981)
54. D.M. Stefanescu, C.R. Loper Jr., Effect of lanthanum and cerium on the structure of eutectic cast iron. Trans. Am. Foundrymen's Soc. **89**, 425–436 (1981)
55. C.M. Dunks, K.B. Turner, Production of compacted graphite iron for brake systems. Trans. Am. Foundrymen's Soc. **89**, 575–586 (1981)
56. C.W. Phillips, Machinability of compacted graphite iron. Trans. Am. Foundrymen's Soc. **90**, 47–52 (1982)
57. D.M. Stefanescu, F. Martinez, Compacted/vermicular graphite cast irons in the Fe–C–Al system. Trans. Am. Foundrymen's Soc. **90**, 39–46 (1982)
58. R.W. Monroe, C.E. Bates, Some thermal and mechanical properties of compacted graphite iron. Trans. Am. Foundrymen's Soc. **90**, 615–624 (1982)
59. W. Simmons, J. Briggs, Compacted graphite irons produced with a cerium–calcium treatment. Trans. Am. Foundrymen's Soc. **90**, 367–379 (1982)
60. S.V. Subramanian, D. Kay, Compacted graphite morphology control. Trans. Am. Foundrymen's Soc. **90**, 589–603 (1982)
61. R.B. Gundlach, The effects of alloying elements on the elevated temperature properties of gray irons. Trans. Am. Foundrymen's Soc. **91**, 389–422 (1983)
62. G.X. Sun, C.R. Loper Jr., Graphite flotation in cast iron. Trans. Am. Foundrymen's Soc. **91**, 841–854 (1983)
63. M. Gagne, R. Goller, Plate fracture in ductile iron castings. Trans. Am. Foundrymen's Soc. **91**, 37–46 (1983)
64. T.R. Farrell, The influence of ASTM Type V graphite form on ductile iron low cycle fatigue. Trans. Am. Foundrymen's Soc. **91**, 61–64 (1983)
65. F. Martinez, D.M. Stefanescu, Properties of compacted graphite iron in the Fe–C–Al system produced by ladle and in-mold treatment. Trans. Am. Foundrymen's Soc. **91**, 593–606 (1983)
66. J. Fowler, D.M. Stefanescu, T. Prucha, Production of ferritic and pearlitic grades of compacted graphite cast iron by the in-mold process. Trans. Am. Foundrymen's Soc. **92**, 361–372 (1984)
67. C.E. Bates, Effects of alloy elements on the strength and microstructure of gray cast iron. Trans. Am. Foundrymen's Soc. **92**, 923–946 (1984)
68. J.P. Hrusovsky, J.F. Wallace, Effect of composition on solidification of compacted graphite iron. Trans. Am. Foundrymen's Soc. **93**, 55–86 (1985)
69. H.H. Cornell, C.R. Loper Jr., Variables involved in the production of compacted graphite cast iron using rare earth-containing alloys. Trans. Am. Foundrymen's Soc. **93**, 435–442 (1985)
70. K.G. Davis, J.G. Magny, D. Hui, Inoculation of permanent mold cast iron. Trans. Am. Foundrymen's Soc. **93**, 939–952 (1985)
71. E.N. Pan, M.S. Lou, C.R. Loper Jr., Effects of copper, tin, and manganese on the eutectoid transformation of graphitic cast irons. Trans. Am. Foundrymen's Soc. **95**, 819–840 (1987)
72. J. Yang, J. Li, R. Li, More powerful inoculants for gray cast iron. Trans. Am. Foundrymen's Soc. **95**, 63–72 (1987)
73. S.B. Singh, A.K. Chakrabarti, A. Basak, Development of low carbon nodular/compacted graphite iron. Trans. Am. Foundrymen's Soc. **97**, 675–684 (1989)
74. D. Glover, C.E. Bates, R. Monroe, The relationships between carbon equivalent, microstructure and solidification characteristics and their effects on strength and chill in gray cast iron. Trans. Am. Foundrymen's Soc. **90**, 745–757 (1982)
75. L.Y. Fang, C.R. Loper Jr., Development of a high modulus graphite cast alloy. Trans. Am. Foundrymen's Soc. **100**, 969–978 (1992)
76. B.V. Kovacs, J.R. Keough, Physical properties and application of austempered gray iron. Trans. Am. Foundrymen's Soc. **101**, 283–291 (1993)
77. T.S. Shih, C.H. Chang, Z.D. Ou, Mechanical properties and microstructures of copper alloyed ADI. Trans. Am. Foundrymen's Soc. **101**, 857–872 (1993)
78. M. Gagne, C. Labrecque, Comparative machinability evaluation of ferritic ductile iron castings. Trans. Am. Foundrymen's Soc. **107**, 537–542 (1999)
79. E. Eleftheriou, C.E. Bates, Effects of inoculation on machinability of gray cast iron. Trans. Am. Foundrymen's Soc. **107**, 659–669 (1999)

80. W.M. Nicola, V. Richards, Age strengthening of gray cast iron, phase I: statistical verification. Trans. Am. Foundrymen's Soc. **107**, 749–756 (1999)
81. R.D. Schelleng, Effect of certain elements on the form of graphite in cast iron. Cast Metals Res. J. **3**(1), 30–38 (1967)
82. G.F. Sergeant, E.R. Evans, Production and properties of compacted graphite irons. Br. Foundrym. **71**(5), 115–124 (1978)
83. K.R. Heimer, Gusseisen mit Vermiculargrahpit and seine Verabeitung zu Zylinderdeckeln Fur Hochleistungs-Diesel-motoren. Geisserei **63**(10), 285–291 (1967)
84. M.J. Lalich, Effects of rare earths on structure and properties of cast iron. Foundry Manag. Technol. **106**(3), 118–119 (1978)
85. AFS Cast Iron Fatigue database (2013)
86. M. König, *Microstructure Formation during Solidification and Solid State Transformation in Compacted Graphite Iron*. Ph.D. Thesis, Chalmers University of Technology (2011)
87. G. Rivera, P.R. Calvillo, R. Boeri, Y. Houbaert, J. Sikora, Examination of the solidification macrostructure of spheroidal and flake graphite cast irons using DAAS and ESBD. Mater. Charact. **59**(9), 1342–1348 (2008)
88. M. Gorny, Solidification of thin wall ductile iron castings with hypereutectic composition. ISIJ Int. **50**(6), 847–853 (2010)
89. E. Fraś, M. Gorny, H.F. Lopez, Eutectic cell and nodule count in gray and nodular cast irons. Mater. Sci. Technol. **23**(9), 1109–1117 (2007)
90. E. Fras, K. Wiencek, M. Gorny, H. Lopez, Theoretical model for heterogeneous nucleation of grains during solidification. Mater. Sci. Technol. **19**(12), 1653–1660 (2003)
91. R. Ruxanda, L. Beltran-Sanchez, J. Massone, D.M. Stefanescu, On the eutectic solidification of spheroidal graphite iron: an experimental and mathematical modeling approach. Trans. Am. Foundry Soc. **109**, 1037–1048 (2001)
92. W.M. Nicola, V. Richards, Age strengthening of gray cast iron phase III-effect of aging temperature. Trans. Am. Foundry Soc. **109**, 1085–1095 (2001)
93. S.C. Lin, T.S. Lui, L.H. Chen, Effect of silicon contents on resonant vibration fracture behavior of ferritic spheroidal graphite cast irons. Trans. Am. Foundry Soc. **109**, 1009–1020 (2001)
94. M. Chisamera, I. Riposan, S. Stan, D. Sparkman, D. Kelley, M. Barstow, Experience producing compacted graphite cast irons by sulfur addition after magnesium treatment. Trans. Am. Foundry Soc. **110**, 851–859 (2002)
95. C.R. Loper, L. Winardi, S. Lekakh, Experiments in pretreatment of ductile irons. Trans. Am. Foundry Soc. **110**, 867 (2002)
96. H. Li, R.D. Griffin, C.E. Bates, Machinability of class 40 gray iron. Trans. Am. Foundry Soc. **110**, 1033–1046 (2002)
97. F.R. Juretzko, L.P. Dix, R. Ruxanda, D.M. Stefanescu, Precondition of ductile iron melts for light weight castings: effect on mechanical properties and microstructure. Trans. Am. Foundry Soc. **112**, 773–786 (2004)
98. J.H. Choi, J.K. Oh, C.O. Choi, J.K. Kim, P.K. Rohatgi, Effect of Bi on formation of microstructure and mechanical properties of ductile iron castings with thin-wall section. Trans. Am. Foundry Soc. **112**, 831–840 (2004)
99. M. Chisamera, I. Riposan, S. Stan, T. Skaland, Effects of residual aluminum on solidification characteristics of un-inoculated and Ca/Sr inoculated gray irons. Trans. Am. Foundry Soc. **112**, 867–878 (2004)
100. D.M. Stefanescu, R.C. Rao, J.W. Woolley, F.R. Juretzko, J.W. Torrance, Production of thin-wall low-nodularity ductile iron through the delayed in-mold process. Trans. Am. Foundry Soc. **113**, 659–668 (2005)
101. M. Popescu, R. Zavadil, J.P. Thomson, M. Sahoo, P. Gassere, Studies to improve nucleation potential of ductile iron when using carbidic ductile iron returns. Trans. Am. Foundry Soc. **115**, 591–608 (2007)
102. R. Khajure, Influence of various process parameters on physical and mechanical properties of ductile iron castings. *Proceedings of the 114th AFS Metalcasting Congress*, Orlando, FL, March 20–23, 2010
103. S. Boonmee, D.M. Stefanescu, Casting skin of compacted graphite iron part II: influence on tensile mechanical properties. Trans. Am. Foundry Soc. **118**, 217–224 (2010)
104. S.N. Lekakh, V.L. Richards, J. Medvedeva, J.M. Murphy, Effect of alloying elements on gray iron natural aging, part 1: manganese. Trans. Am. Foundry Soc. **119**, 379–388 (2011)
105. S. Grenier, C. Labrecque, Microstructure, composition and impact strength variations measured in a heavy section as cast ferritic ductile iron casting. Trans. Am. Foundry Soc. **120**, 263–275 (2012)
106. E.N. Pan, C.C. Lin, R.M. Chang, Optimal alloy design and process conditions for heavy section ductile cast irons with high sub-zero impact toughness. Trans. Am. Foundry Soc. **120**, 289–296 (2012)
107. P. Larrañaga, J. Sertucha, A. Loizaga, R. Suárez, D.M. Stefanescu, Gray cast iron with high austenite-to-eutectic ratio part III—high strength, low hardness, high carbon equivalent gray iron with superfine graphite. **120**, 347–353 (2012)
108. D.M. Stefanescu, M. Moran, S. Boonmee, W.L. Guesser, Use of combined liquid displacement and cooling curve analysis in understanding the solidification of cast iron. Trans. Am. Foundry Soc. **120**, 365–374 (2012)

109. P. Larranaga, J. Sertucha, A. Loizaga, R. Suarez, D.M. Stefanescu, Effect of carbon equivalent and alloying elements on the tensile properties of superfine interdendritic graphite irons. Trans. Am. Foundry Soc. **120**, 347–353 (2012)
110. W.C. Jeffery, E.E. Langner, W.G. Mitchell, G.D. Azizi, Relationship of carbon equivalent to the properties of cast iron. Trans. Am. Foundrymen's Soc. **62**, 568–578 (1954)
111. S. Biswas, C. Monroe, T. Prucha, Analysis of published cast iron experimental data, in *Proceedings of the 3rd World Congress on Integrated Computational Materials Engineering (ICME)* (Wiley, 2015), pp. 293–303
112. Automotive Gray Iron Castings. J431_200012, Society of Automotive Engineers (SAE)
113. ASTM Standard A842-11a, Standard Specification for Compacted Graphite Iron Castings (ASTM International, West Conshohocken, PA, 2011). www.astm.org
114. ASTM Standard A536-64, Standard Specification for Ductile Iron Castings (ASTM International, West Conshohocken, PA, 2009). www.astm.org
115. S. Jura, H. Borek, J. Sakwa, Differential analysis of the process of cast iron solidification, in *46th International Foundry Congress*, Madrid, Spain (1979)
116. S. Hua-Qin, W. Qigui, S. Hongqing, G. Xinli, Latest developments in production and research works of gray cast iron in China. Trans. Am. Foundrymen's Soc. **99**, 363–367 (1991)
117. Y. Yang, A. Louvo, T. Rantala, Effect of alloying and cooling rate on the microstructure and mechanical properties of low-alloy gray iron, in *57th World Foundry Congress*, September (1990), pp. 23–28
118. C.E. Bates, J.R. Tucker, H.S. Starrett, Composition, section size and microstructural effects on tensile properties of pearlitic gray cast iron. AFS Research Report No. 5, Sep 1991
119. I.L. Svensson, M. Wessen, A. Gonzalez, Modeling of structure and hardness in nodular cast iron castings at different silicon contents, in *Proceedings of Modeling of Casting; Welding and Advanced Solidification Process VI, TMS*, ed. by T.S. Piwonka, V. Voller, L. Katgerman (1993), pp. 29–36